Rock slope assessment in tropical climates: A comparative study using multiple rock mass classification system

AHMAD FAIZ SALMANFARSI, HARYATI AWANG*

Faculty of Civil Engineering Technology, Universiti Malaysia Pahang Al-Sultan Abdullah, Lebuhraya Tun Razak, 26300 Kuantan, Pahang, Malaysia

* Corresponding author email address: haryatiawang@umpsa.edu.my

Abstract: In tropical climates, exposed rock slopes are significantly weathered to form extensive weathering profiles. Combined with other factors such as slope orientation, discontinuities, and weather conditions, rock slope conditions need to be monitored for potential instability and failures. Rock mass classification is one of the most widely used empirical methods of classifying rock mass slope properties. Several rock mass classifications have been developed each year based on different rock mass parameters. This paper evaluated various cut rock slopes along Karak-Lanchang, Pahang, which showed potential failure zones from discontinuity sets and weathering zones, using selected rock mass classification systems. The rock slope mapping was carried out using conventional field mapping and Terrestrial Laser Scanning (TLS). Comparison between the mapped discontinuities and the discontinuities extracted from TLS revealed some degree of correlation. From the discontinuities mapping, kinematic analysis identified several potential slope failure modes. The stability conditions of the slopes were determined, and a comparative analysis of the different rock mass classifications was carried out. The paper highlights the significance of the classification results and discusses the contributing factors that affected the results of the various classifications. A more comprehensive classification of rock slopes is presented in this paper by comparing the results obtained from the different rock mass classifications.

Keywords: Rock mass classification, kinematic analysis, TLS, granite, engineering geology

Abstrak: Dengan iklim tropika, cerun batu yang terdedah mengalami proses luluhawa dengan ketara, justeru menghasilkan profil luluhawa yang meluas. Digabungkan dengan faktor lain seperti orientasi cerun, ketakselanjaran, dan keadaan cuaca, terdapat keperluan untuk memantau keadaan cerun batuan untuk potensi ketidakstabilan dan kegagalan perlu dilakukan. Pengelasan jasad batuan adalah salah satu kaedah empirikal yang paling banyak digunakan bagi mengklasifikasikan sifat jasad cerun batuan. Beberapa pembangunan sistem pengelasan jasad batuan telah dilakukan, berdasarkan kepada beberapa parameter jasad batuan yang berbeza. Di dalam kertas kajian ini, beberapa cerun batu di sepanjang jalan Karak-Lanchang, Pahang, yang menunjukkan zon berpotensi mengalami kegagalan pengaruh daripada set ketakselanjaran dan zon luluhawa, telah dinilai menggunakan sistem pengelasan jasad batuan yang terpilih. Pemetaan cerun batuan dilakukan menggunakan pemetaan lapangan konvensional, serta pemetaan menggunakan Terrestrial Laser Scanning (TLS). Perbandingan antara ketakselanjaran daripada pemetaan lapangan dan ketakselanjaran yang diproses daripada pemetaan TLS menunjukkan terdapat korelasi di antara dua data tersebut. Analisis kinematik telah mengenalpasti beberapa potentsi untuk mod kegagalan cerun, berdasarkan kepada data pemetaan ketakselanjaran. Kesestabilan cerun dikenal pasti, dan analisis perbandingan antara sistem pengelasan jasad batuan yang berbeza telah digunakan. Kertas kajian ini menunjukkan kepentingan hasil dari pengelasan, dimana faktor yang mempengaruhi hasil pengelasan dibincangkan. Pengelasan cerun batuan yang lebih komprehensif berdasarkan perbandingan hasil analisis antara pengelasan jasad batuan yang berbeza dibentangkan dalam kertas kajian ini.

Kata kunci: Pengelasan jasad batuan, TLS, granit, geologi kejuruteraan

INTRODUCTION

Malaysia's topography consists of many mountains and highlands, with developments such as high-rise buildings and the construction of roads and highways taking place along these bodies of rocks. With the continuous depletion of low-lying areas for development, more rock slopes are being excavated to make way for development. This exposes more and more people to the risk of slope failures. Over

recent years, slope failures have become frequent, and they are one of the most destructive natural disasters besides flooding (Abdul Rahman & Mapjabil, 2017). Slope failures over constructed slopes significantly endanger human lives and economic development, especially where highways are involved (Awang *et al.*, 2021b; Zaini *et al.*, 2022). Although failures of rock slopes that have weathered to form residual soil are common in equatorial conditions such as those in

Malaysia, the geological properties of the slopes (i.e., the underlying rock unit and geological structures) are still a significant cause of landslides, having been reported as the main contributing factor to landslides worldwide (Highland & Bobrowsky, 2008; Public Work Department, 2009). A rock mass is heterogeneous and anisotropic, consisting of discontinuities that are produced from stresses due to tectonic activities or weathering effects (Nagendran et al., 2019). An improper understanding of this complexity may lead to rock slopes failing repeatedly, even though protection measures may have been applied to these problematic slopes. Several case studies reveal highways and roads in Malaysia which repeatedly fail, despite the use of slope protection measures, suggesting the latter are incorrect and the result of a lack of proper understanding of the underlying rock unit and geological features of the slopes (Tan, 2017).

Given the concerns about slope stability, several methods are available for evaluating it. Generally, these are divided into kinematic analysis, limit equilibrium, numerical modelling, and empirical methods (Basahel & Mitri, 2017). Kinematic analysis has been a staple for the majority of rock slope analysis by practitioners in Malaysia, where engineering studies of rock slopes are based on measurement and analysis of discontinuities by stereographic projection (Tan, 2017). The technique uses a discontinuity orientation projection by pole, which depicts the dip and the dip direction of the joint on a 2D stereonet (Price & Cosgrove, 1990). Case studies of previously published rock slope stability assessments in Malaysia by Abdul Rahim et al. (2023) show a prevalence of kinematic analysis, with stability rating and numerical analysis being two other commonly used methods.

Rock mass classifications fall under the empirical method and are among Malaysia's most commonly used assessments of rock slope stability. They were initially developed for underground excavations to design underground projects (Bieniawski, 1993; Hoek, 2007). Rock mass classification ratings have been developed from several parameters, including numerical values and weighing factors, whereby an empirical formula was derived from the weighing values to obtain a final rating for a rock mass (Hack et al., 2003). In subsequent studies, this classification system was applied by calibrating relevant parameters for surface excavation, making it applicable to classifying cut slopes (Pantelidis, 2009). Rock mass classifications have continued to be used due to their simplicity and capacity to manage uncertainty (Anbazhagan et al., 2017). Recently, several researchers have carried out comparative analysis using rock mass classifications (Basahel & Mitri, 2017; Kundu et al., 2017; Sardana et al., 2019; Khanna & Dubey, 2021), proving the validity of this method for rock slope stability analysis.

Although the parameters for rock mass stability analysis and classification are commonly obtained through conventional field mapping, developments in remote sensing, such as Structure from Motion (SfM), photogrammetry,

and Light Detection and Ranging (LiDAR), have led to the integration of these methods into the mapping of rock mass surfaces. One application of LiDAR for rock slope mapping is the Terrestrial Laser Scanning (TLS), which is among the methods available to extract rock mass discontinuity automatically using three-dimensional models (Battulwar et al., 2021). These techniques have been used for discontinuity extraction in rock mass classification (Riquelme et al., 2016; Papathanassiou et al., 2020), and they are used to complement manual data collection where physical access is impossible (Bordehore et al., 2017). Examples of local studies utilising TLS for discontinuity extraction for rock mass characterisation include the works by Hellmy et al. (2019), Roslan et al. (2019), and Ismail et al. (2022). Romana et al. (2015) briefly reviewed the application of the photogrammetric technique and LiDAR in relation to the development of rock mass classifications, indicating that these techniques can be utilised to obtain parameters relevant to rock mass classification. Their application means that the kinematics and rock mass classification of rock slopes can be calculated from discontinuity extraction through TLS or other remote sensing methods. Implementing these methods would be an improvement by not only making rock slope assessment convenient and fast but also improving the assessment quality (Abdul Rahim et al., 2023).

This study aimed to conduct a comparative analysis of the classification of the rock slopes in the study area. For that purpose, discontinuity mapping of the rock slopes was carried out using both conventional field mapping and TLS mapping. Kinematic analysis of the slopes was conducted to identify the most likely mode of failure. Then, several different rock mass classifications were chosen: the original Rock Mass Rating (RMR) (RMR_{so}) (Bieniawski, 1973; 1976; 1979; 1989); the continuous function RMR, otherwise known as the Modified-RMR (M-RMR) (Sen & Sadagah, 2003); the 2014 RMR update (RMR₁₄) (Celada *et al.*, 2014), the original Slope Mass Rating (SMR) (Romana, 1985); the continuous function SMR (CSMR) (Tomás et al., 2007); the graphical SMR (GSMR) (Tomás et al., 2012); the Q-slope system, shortened to the Q-slope (Barton & Bar, 2015); the original Geological Strength Index (GSI), otherwise known as GSI₉₅ (Hoek et al., 1995); the 2002 quantification of GSI (GSI₀₂) (Sonmez & Ulusay, 2002); the 2013 quantification of GSI (GSI₁₃) (Hoek et al., 2013); the Slope Stability Rating (SSR) (Taheri & Tani, 2010); and the Hazard Index (HI) (Pantelidis, 2010). The rock mass classification and stability analysis of the slopes produced using these methods were then examined for their validity, and the slope classification and stability categories were compared.

STUDY AREA

The study area comprises three rock slopes along the Karak-Lanchang section. The study area passes through the Central Belt of Peninsular Malaysia, where Carboniferous to Permian aged sedimentary and metasedimentary rocks dominate the geology, along with Triassic interbedded sedimentary rocks and volcanics, Jurassic continental sedimentary deposits, and granitic bodies. The reported rock units along the highway include the Tembeling Group, Semantan Formation, and Seri Jaya Beds, as well as volcanic and granitoid types (Simon *et al.*, 2008; Tan *et al.*, 2008).

The study was focused on the rock mass characteristics of the granitic rock slopes (Figure 1). The selected slopes are large granitic slopes that are not covered with significant protection such as shotcrete or rock mesh. They are structurally controlled, i.e. exhibiting discontinuity sets, which may trigger potential failures (Awang et al., 2021a). These granites are part of the Eastern Belt of Peninsular Malaysia granitoids, which are predominantly of the I-type and range widely in age from the Permian to the Triassic and Upper Cretaceous (Gasparon & Varne, 1995). In Kuantan, the granite is an isolated pluton of the I-type of fractionated hornblende biotite granite of the Late Permian age. The area's granite is graded, ranging from coarse-grained, primary textured equigranular to porphyrytic biotite and hornblende granite (Cobbing et al., 1992). Biotite granite is reported to comprise most of the granite, which consists of mediumgrained to coarse-grained rock with a subhedral-granular texture, which is made up of quartz, K-feldspar, plagioclase, muscovite, and biotite (Schwartz et al., 1995). Recent studies on the granite of Pahang relate to its role as a parent rock for bauxite (Nugraheni et al., 2018) and the concentration of rare earth elements in weathered granite (Ghani et al. 2019).

METHODOLOGY

Study site and procedure for field data collection

Three slopes were selected for the discontinuity mapping and stability analysis using kinematic and rock mass classifications. The basic features of the slopes are summarised in Table 1, with the scanline lengths along the slope surface noted. An overall view of the rock slopes examined in this study is shown in Figure 2.

Geological mapping was carried out by implementing the scanline method, which involves using measurement tape along the length of cut rock slopes and keeping the tape as flat as possible along the slope's surface. Measurement and observation along the scanlines were recorded with the starting point of the lines. GPS measurements were taken for each end of the scanlines, where the coordinates and elevations were recorded. The rock types were identified visually for each scanline, using reference charts for grain size, colour, and texture. Photographs and field notes of the slope area were taken, and weathering profiles were also noted alongside the rock units. The weathering

Table 1: Summary of basic features of studied slopes.

Site	Slope height	Slope dip/dip direction	Scanline length
Site 1	21 m	70°/140°	68.3 m
Site 2	28 m	70°/155°	37.5 m
Site 3	18 m	66°/330°	57.7 m

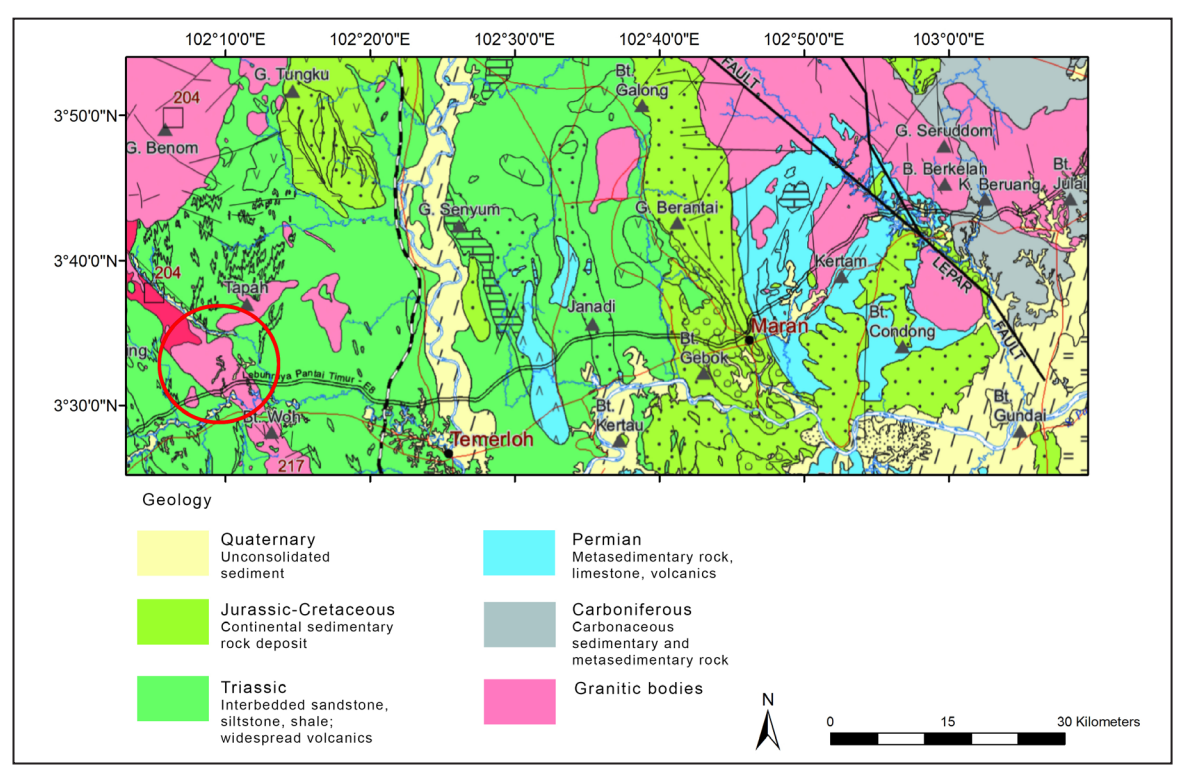


Figure 1: Geological rock unit along the Lanchang-Karak area, with the studied slopes highlighted in a red circle. Geology modified from Tate *et al.* (2008).

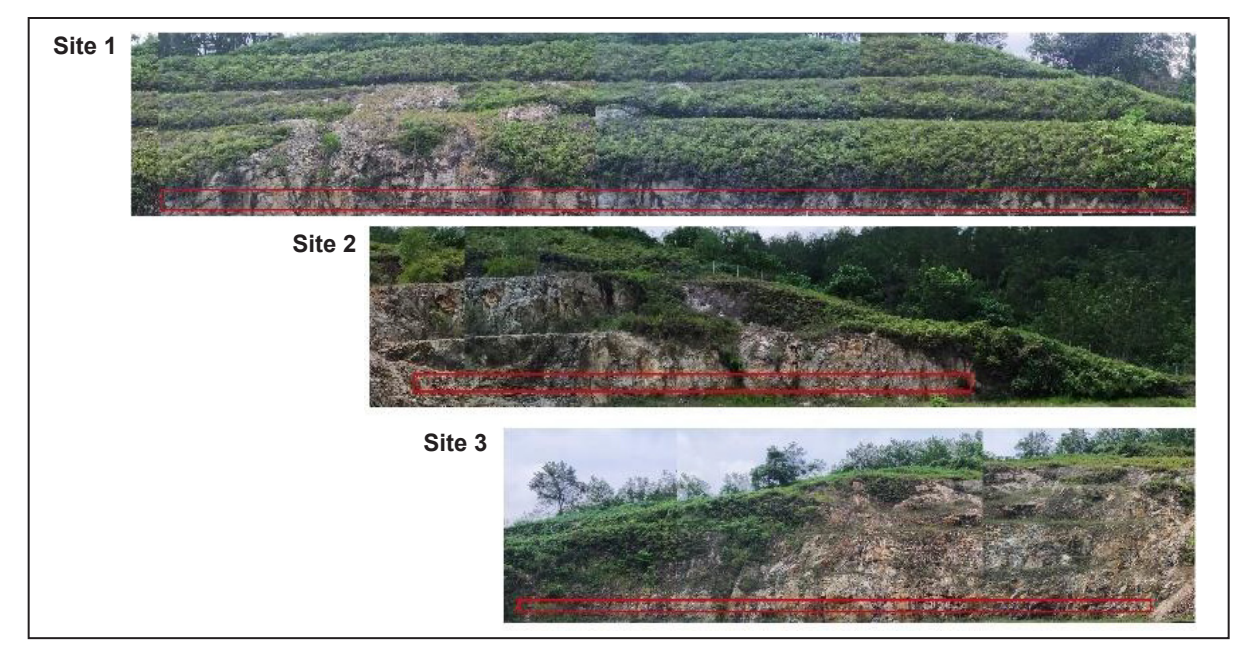


Figure 2: Overview of the rock slopes examined in this study, with the alignment of the scanlines.

mapping used the measurements from a Schmidt Rebound Hammer, which notes the value of the rebound hammer for the different weathering grades of the rock surface. For discontinuity mapping, several parameters relevant to rock mass classification were measured: the type of discontinuity, dip and dip direction, length/persistence, width/aperture, weathering, spacing, condition of joint surface, and presence of water. Finally, the slope geometry (i.e., the height, dip, and dip direction) was measured.

The mapping process of the geologic unit and discontinuity followed the British Standards Institution (BSI) (2018) standard. The weathering condition of the cut slopes was investigated following the BSI standard (2015). In addition, the classifications by the ISRM (Komoo, 1995; Fookes, 1997; Ulusay & Hudson, 2007) were also adopted during field mapping to enable more accurate descriptions of the weathering grade of the granite in the field.

TLS mapping and discontinuity extraction

A laser scanning survey is a remote sensing method used to supplement conventional methods for measuring and recording discontinuities on rock slopes. The terrestrial laser scanning (TLS) method was chosen for discontinuity extraction from the surfaces of the cut slopes. The scanner produces a point cloud with which a highly detailed 3D terrain model can be constructed.

The slope surfaces were scanned using a single Teledyne Optech Polaris TLS unit. The TLS survey was carried out by following the methods suggested by the ISRM for using 3D laser scanning for rock mechanics and rock engineering applications (Ulusay, 2015). The control targets of the rock slope were registered by following the methods suggested and tested by Sturzenegger & Stead (2009). In this study,

data registration was carried out using the scanner, which accurately measures the orientation of discontinuities from the slope. At each study site, the rock slopes were measured from several control points or stations to obtain more comprehensive slope views and avoid occlusions. Varying degrees of horizontal and vertical views of the slopes were measured at each station. The TLS middle range performance is up to 40 m for a detailed scan and up to 350 m for the standard scan. Several control points were used to scan the slope surfaces. The scanning time for each station was estimated as 8 to 30 minutes. The scanned rock slope surfaces were then registered before the point cloud data were processed.

At each site, the control points for TLS were identified, with the instrument set up on a known point using a combination of tripod and tribrach before being levelled using an electronic bubble on its onboard interface. The instrument took GPS measurements internally at the start of each scanning procedure. The scanning process followed the setting up of the survey parameters: the horizontal field of view (HFOV), vertical field of view (VFOV), range, and scan density. Upon completion of the TLS surveying, the measured point cloud data were processed using the ATLAScan software.

The next step was the extraction of discontinuities sets from the point cloud data using the Discontinuity Set Extractor (DSE) software developed by Adrián Riquelme (Riquelme *et al.*, 2014) to extract discontinuities set from the point clouds of the rock mass. The normal vectors of the point clouds were calculated using the known algorithm and the Kernel Density Estimation method (Botev), whereby each point of the point cloud was assigned to a group of planes, which were subsequently grouped into discontinuity sets.

Laboratory testing

Selected samples of rock mass from the slopes were collected for physico-mechanical tests, which included point load strength (PLS) tests, uniaxial compressive strength (UCS) tests, slake durability, and friction angle tests. For both the PLS and UCS tests, the procedures were conducted according to the method suggested by the ISRM (Ulusay & Hudson, 2007; Ulusay, 2015). The friction angles of the samples were determined from tilt tests, following the steps outlined by the ISRM (Alejano *et al.*, 2018).

Kinematic analysis

After mapping the discontinuities – using either scanline mapping or TLS mapping - the next step was to carry out kinematic analysis. Discontinuities readings were analysed using the DIPS software (Rocscience Inc., 2014), whereby the potential rock failure for the discontinuities sets can be calculated using the Markland Test principle (Hoek & Bray, 1981). A visualisation of the discontinuities and structural data using stereonet techniques was made available, and other computational features were carried out, such as statistical contouring of orientation clustering, mean orientation and confidence estimation, cluster variance, kinematic analysis, and qualitative and quantitative attribute analysis. The likelihood and potential for the different failure modes (planar, wedge, and topping) could then be determined. The failure potential of each slope was used in the calculation for the rock mass classification of the SMR, Q-slope, and HI.

Rock mass classification

As mentioned previously, several different rock mass classifications were utilised in this study. The parameters of each classification are as follows:

The original Rock Mass Rating (RMR), or RMR₈₉ (Bieniawski, 1973; 1976; 1979; 1989), is calculated using five parameters: the strength of the intact rock material (uniaxial compressive test (UCS) or point load strength (PLS)) (R₈), rock quality designation (R_{RQD}), spacing between discontinuities (R_{SD}), condition of discontinuities (R_{CD}), and groundwater condition (R_{CG}). The RMR₈₉ equation is shown as Eq. 1.

$$RMR_{89} = R_{\delta} + R_{ROD} + R_{SD} + R_{CD} + R_{CG}$$
 (1)

The continuous function RMR, or the Modified-RMR (M-RMR) (Sen & Sadagah, 2003), uses the same parameters as the RMR₈₉. However, instead of ranking the parameters based on the user's experience and selecting the discrete values as the original RMR does, the classification uses the continuous rating function of the RMR₈₉. The classification calculation applies to either the PLS reading (Eq. 2) or the UCS reading (Eq. 3) of selected rock samples taken from slopes.

M-RMR =
$$0.2(RQD) + 15log(SD) + 1.670_{\delta} + 2.9log$$

(Groundwater flow) + $35.67 + R_{CD}$ (2)

M-RMR =
$$0.2(RQD) + 15log(SD) + 0.075_{\delta} + 2.9log$$

(Groundwater flow) + $34.00 + R_{CD}$ (3)

The 2014 RMR update (RMR14) (Celada *et al.*, 2014) combines the R_{RQD} and R_{SD} parameters of RMR₈₉ to form the density of discontinuities (RDD), modifies the rating for RCD (R_{CD14}), and adds a new parameter, the intact rock alterability rating (R_{IRA}), using the values from Slake Durability tests. The RMR₁₄ equation is shown as Eq. 4.

$$RMR_{14} = R_{\delta} + R_{DD} + R_{CD14} + R_{IRA} + R_{CG}$$
 (4)

The original Slope Mass Rating (SMR) (Romana, 1985) adds the adjustment factors F_1 , F_2 , F_3 , and F_4 to the reading of the original RMR, where F_1 is an adjustment factor based on the parallelism between the joint strike (α_j) (or the plunge direction of the intersection line of two planes (α_i)) and the slope face strike (αs) ; F_2 refers to the joint dip angle (βi) in planar failure, or the plunge of the intersection line of two planes (β_i) in wedge-type failure mode; F_3 reflects the effect of the angle between the slope face dip (βs) and the joint dip (βi) , or the plunge of the intersection line of two planes (βi) ; and F4 is an adjustment factor based on the excavation method used on the slope. The SMR equation is shown as Eq. 5.

$$SMR = RMR + F_1 F_2 F_3 + F_4$$
 (5)

The continuous function SMR (CSMR) (Tomás *et al.*, 2007) uses the same formula as the original SMR, with the modification that the F_1 , F_2 , and F_3 factors are calculated using continuous functions, as opposed to the discrete rating used in the original SMR. The calculations for each factor are shown in Eq. 6 – Eq. 9.

 $F_1 = (16/25) - (3/500) \arctan[(1/10) (|A|-17)]$ (6) where $|A| = |\alpha_j - \alpha_s|$ for planar failure mode, or $|\alpha_j - \alpha_s|$ for toppling failure mode, or $|\alpha_i - \alpha_s|$ for wedge failure mode.

 $F_2 = (9/16) + (1/195) \arctan[(17/100) (B-5)]$ (7) where B = dip angle of the joint, β_j for planar or toppling failure mode, or the plunge of the intersection line of two planes, β_i for wedge failure mode.

$$F_3 = -30 + (1/30) \arctan C$$
 (8)

where C = difference in angle between the joint dip and slope dip, $\beta_{j} - \beta_{s}$ for planar failure mode, or the difference in angle between the plunge of the intersection line of two planes and slope dip, $\beta_{i} - \beta_{s}$ for wedge failure mode. For toppling failure, the FS calculation is shown in Eq. 9:

$$F_3 = -13 + (1/7) \arctan (C-120)$$
 (9)
where C = sum of the two dip angles of the joint and slope, $\beta_i - \beta_c$.

The graphical SMR (GSMR) (Tomás *et al.*, 2012) combines the F_1 and F_2 parameters under the parameter Ψ , with both the Ψ and F_3 parameters determined graphically using stereo plots. The GSMR equation is shown as Eq. 10:

$$SMR = RMR + \Psi F_3 + F_4 \tag{10}$$

The Q-slope system, or Q-slope (Barton & Bar, 2015), uses the RQD parameter from RMR₈₉, as well as other parameters related to the discontinuity condition: the number of joint sets (J_n), joint roughness number for critically oriented joint sets (J_n), joint alteration number for critically oriented joint sets (J_a), discontinuity orientation factor (O), environmental and geological condition number (J_{wice}), and stress reduction factor that considers in situ stresses and observed slope conditions (SRF_{slope}). The Q-slope equation is shown as Eq. 11.

$$Q-slope = [RQD/J_n][(J_r/J_a)O][J_{wice}/SRF_{slone}]$$
(11)

The original Geological Strength Index (GSI), or GSI_{95} (Hoek *et al.*, 1995), can be quantified from the RMR₈₉ value using the equation shown as Eq. 12.

$$GSI_{95} = RMR_{89} - 5 \tag{12}$$

The 2002 quantification of GSI (GSI₀₂) (Sonmez & Ulusay, 2002) is derived from a graphical plotting of two indices: the Surface Condition Rating (SCR), derived from rating the roughness, weathering, and infilling of joints, or R_r, R_w, R_f; and the Structure Rating (SR), derived from the volumetric joint count, Jv. The equations for calculating SCR and SR are shown as Eq. 13 and Eq. 14.

$$SCR = R_r + R_w + R_f \tag{13}$$

$$SR = -17.5 \ln(J_{y}) + 79.8 \tag{14}$$

The 2013 quantification of GSI (GSI₁₃) (Hoek *et al.*, 2013) is derived from the RQD and joint condition parameters (R_{CD}) of RMR₈₉. The GSI13 equation is shown as Eq. 15.

$$GSI_{13} = 1.5R_{CD} + RQD/2$$
 (15)

The Slope Stability Rating (SSR) (Taheri & Tani, 2010) uses the value of GSI_{02} , as well as additional parameters not found in most of the aforementioned classifications: the UCS (P_1), rock type (P_2), slope excavation method (P_3), groundwater condition (P_4), and earthquake force (P_5). The SSR equation is shown as Eq. 16.

$$SSR = GSI + P_1 + P_2 + P_3 + P_4 + P_5$$
 (16)

The Hazard Index (HI) (Pantelidis, 2010) is based on two main parameters: the normal condition factor (f_{NC}) ,

which is based on the potential mode of failures of rocks or, in the case of non-structurally controlled slopes, the GSI classification; and the triggering mechanism for failure (f_{TM}) , which is based on the annual precipitation and the drainage factor of the slope cutting. The HI equation is shown as Eq. 17:

$$HI = (f_{NC}f_{TM})^{1/2}$$
 (17)

RESULTS AND DISCUSSION Geological and physico-mechanical properties

The ranges of the physical properties of each site are given in Table 2. The representative weathering grade of the rock slope was used as input in the subsequent kinematic analysis and rock mass classifications. A discussion of the readings is given below.

For Site 1, the mapped granite is light grey in colour, with a weathered portion showing brownish-red to yellowish-brown colour. The granite of the site is rather fine-grained, with the quartz being the most identifiable mineral in hand specimens. Based on the Schmidt Rebound Hammer mapping and field identification, most slopes were weathered to Grade II.

For Site 2, the mapped granite is light grey in colour, with the weathering forming reddish-brown to brownish-orange material. The granite of the site is generally fine-grained, with quartz being the most identifiable mineral in hand specimens. Large traces of faults could be found cutting across the eastern part of the slope. Dark fine-grained igneous veins could be found cutting across the centre section of the slope. Fine weathered soil could be found across several toe sections of the slope, which appears to be debris from previous slope failures. Based on the Schmidt Rebound Hammer mapping and field identification, the majority of the slopes were weathered to Grade III.

For Site 3, the mapped granite is light grey in colour, with the weathered portion showing a brownish-orange colour. The granites are fine-grained, with quartz grains being the most identifiable mineral on hand specimens. Several large traces of faults could be found cutting across the granite body, especially on the centre of the exposed slope. The top of the slopes is weathered to form a greyish-brown soil layer. Based on the Schmidt Rebound Hammer mapping and field identification, the majority of the slopes were weathered to Grade II.

Discontinuity mapping

The mapped discontinuities set from Sites 1 to 3 is summarised in Table 3, and the extracted discontinuity from TLS and the stereoplot of discontinuity sets from Sites 1 to 3 are summarised in Figures 3 and 4, respectively. The mapped discontinuity sets for each slope are discussed below.

For Site 1, six major sets of discontinuities (J1-J6) were identified from scanline mapping, and seven major sets of discontinuities (J1–J7) were identified from TLS mapping.

Table 2: Summary of weathering and physico-mechanical properties of Site 1-Site 3.

Properties	Slope	Mean	Min	Max	Standard deviation
Schmidt	Site 1	50.6	41.2	64.6	7.60
Rebound	Site 2	36.2	27.6	41	4.60
Hammer	Site 3	55.3	45.8	64	5.12
Point Load	Site 1	4.15	1.56	7.40	2.70
Strength, PLS	Site 2	1.19	0.20	3.80	0.86
(MPa)	Site 3	5.44	2.95	11.36	1.75
Uniaxial	Site 1	89.08	71.27	100.06	13.31
Compressive Strength, UCS	Site 2	87.31	85.77	88.84	2.17
(MPa)	Site 3	81.69	68.31	91.49	10.46
Slake	Site 1	99.13	98.74	99.44	0.26
durability	Site 2	96.54	94.56	98.10	1.50
index, Id ₂ (%)	Site 3	99.05	97.62	99.61	0.54
	Site 1	33	26	40	
Tilt test	Site 2	31	28	34	
	Site 3	33	30	40	

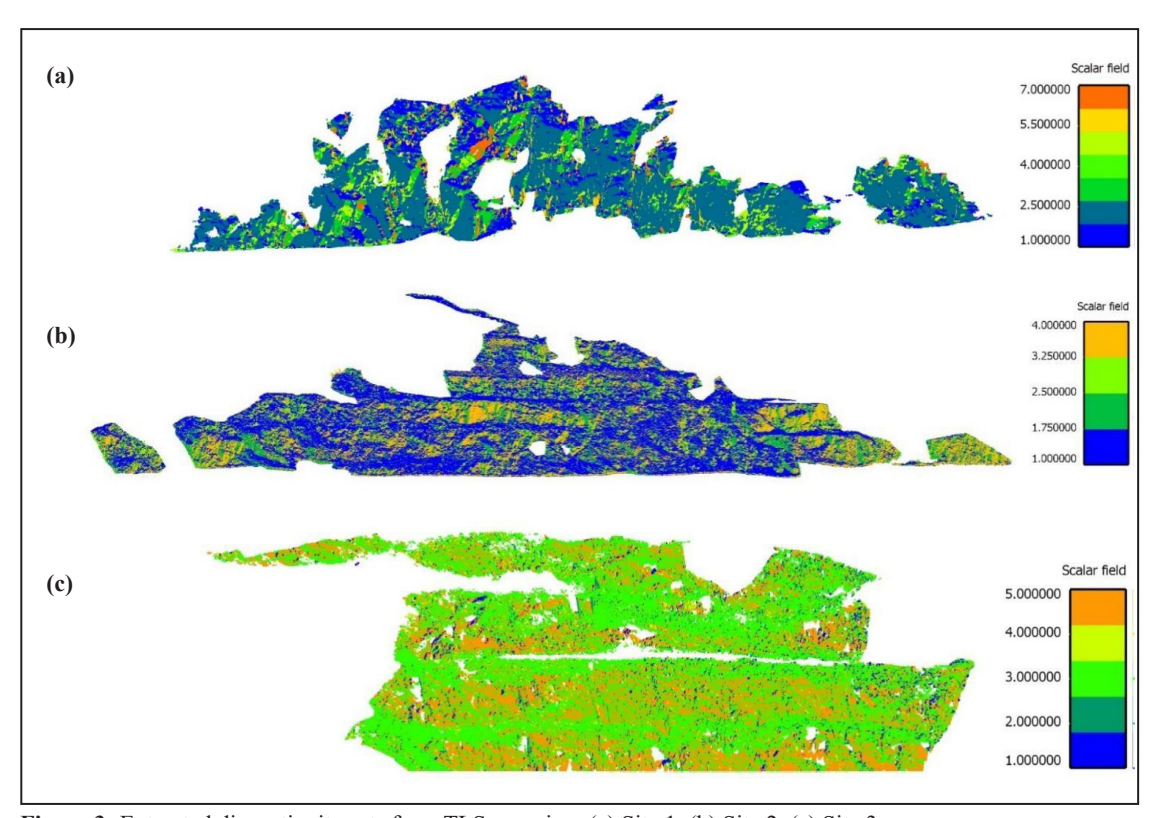


Figure 3: Extracted discontinuity sets from TLS mapping: (a) Site 1, (b) Site 2, (c) Site 3.

AHMAD FAIZ SALMANFARSI, HARYATI AWANG

Table 3: Value of discontinuities set for Site 1-Site 3.

Site 1	Scanline mapping	Dip (°)	Dip direction (°)	%
	J1	31.43	050.51	22.08
	J2	77.82	063.6	13.75
	Ј3	78.00	091.63	11.25
	J4	79.18	181.81	12.5
	J5	81.27	221.66	13.33
	Ј6	71.68	262.76	20
Site 1	TLS mapping	Dip (°)	Dip direction (°)	%
	J1	34.51	032.48	17.46
	J2	80.36	049.57	55.12
	Ј3	86.19	172.68	5.60
	J4	13.80	191.19	1.95
	J5	64.59	199.77	5.08
	Ј6	85.72	271.48	4.49
	J7	67.94	312.18	3.33
Site 2	Scanline mapping	Dip (°)	Dip direction (°)	%
	Л1	75.23	033.46	34.87
	J2	33.82	054.09	14.47
	Ј3	88.50	074.13	5.263
	J4	77.71	178.28	4.61
	J5	54.85	275.47	4.61
Site 2	TLS mapping	Dip (°)	Dip direction (°)	%
	J1	32.10	155.56	28.42
	J2	90	188.47	9.61
	J3	90	278.47	9.85
	J4	87.10	337.93	10.98
Site 3	Scanline mapping	Dip (°)	Dip direction (°)	%
	J1	73.17	044.92	41.03
	J2	55.54	135.31	13.10
	J3	71.19	252.88	23.10
Site 3	TLS mapping	Dip (°)	Dip direction (°)	%
	J1	70.77	050.44	4.40
	J2	90	079.16	6.41
	J3	40.02	191.32	35.36
	J4	68.51	323.53	5.00

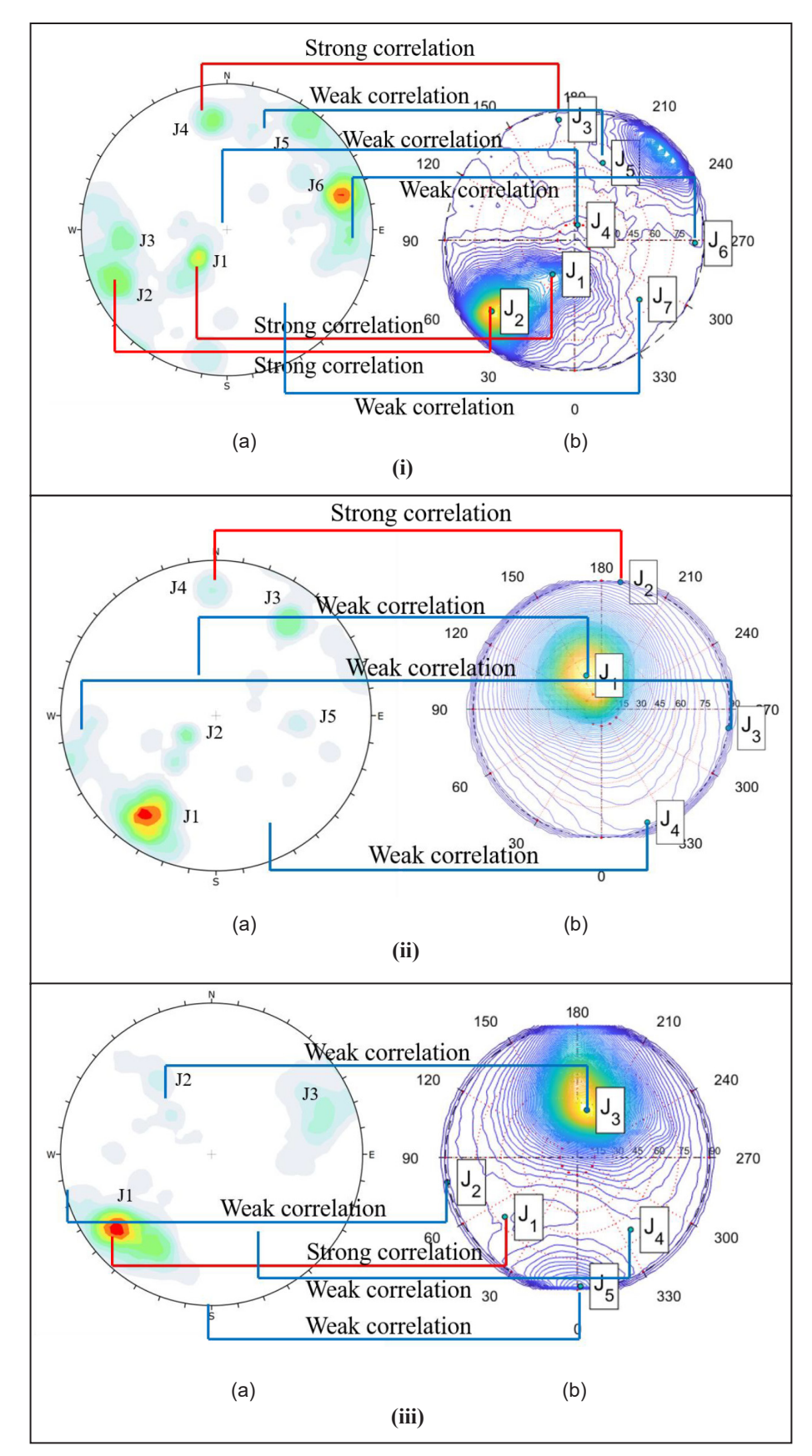


Figure 4: Stereographic projection of discontinuity sets for: (i) Site 1, (ii) Site 2, (iii) Site 3; (a) scanline mapping, (b) TLS mapping.

A stereographic projection of the mapped discontinuities from both the scanline and TLS mapping shows that three discontinuity sets are strongly correlated with the scanline survey and four discontinuity sets are weakly correlated.

For Site 2, five major sets of discontinuities (J1-J5) were identified from scanline mapping, and four major sets of discontinuities (J1-J4) were identified from TLS mapping. A stereographic projection of the mapped discontinuities from both the scanline and TLS mapping shows that one discontinuity set is strongly correlated with the scanline survey. In contrast, three discontinuity sets are weakly correlated.

For Site 3, three major sets of discontinuities (J1-J3) were identified from scanline mapping, and five major sets of discontinuities (J1-J5) were identified from TLS mapping. A stereographic projection of the mapped discontinuities from both the scanline and TLS mapping shows that one discontinuity set is strongly correlated with the scanline survey. In contrast, four discontinuity sets are weakly correlated.

The results of the comparative correlation between the scanline and TLS mapping indicate a varying degree of correlation between the discontinuity sets mapped by the two methods. This discrepancy has also been reported by Hellmy et al. (2019), where the vegetation coverage on the slope surface and the weathering of rock material were cited as possible explanations for the differences in the distribution of the plotted discontinuity sets for TLS mapping in comparison to the field mapping of the discontinuity sets. The vegetation obscured the discontinuity from being picked up by TLS mapping. In the subsequent analysis, only the discontinuity sets from TLS were used in the kinematic analysis and SMR analysis of the slopes because the discontinuity set mapping using TLS did not yield the discontinuity set parameters necessary for the analysis of rock mass classifications.

Kinematic analysis

The kinematic analysis results for each slope are shown in Figure 5 and summarised in Table 4. For Site 1, the potential for planar, wedge, and toppling failure is significant, according to scanline mapping; and the potential for wedge and toppling failure is significant according to TLS mapping. For Site 2, the potential for wedge and toppling failure is significant according to scanline mapping; and the potential for planar, wedge, and toppling failure is significant according to TLS mapping. For Site 3, the potential for wedge and toppling failure is significant according to scanline mapping; and the potential for wedge failure is significant according to TLS mapping.

From the tabulated results for the kinematic analysis using both the conventional scanline method and TLS mapping, the results indicate that where the rock slopes are visible and there is little covering of other elements such as vegetation or fill materials, the kinematic potential

mode of failure obtained by the two methods is comparable. However, in the case of Site 2, where the slopes are heavily weathered and the weathered material covers a large portion of the slopes, the discontinuity sets extracted from TLS produced an orientation of discontinuity sets that are steep in their dip values, as observed in Figure 4(b), which is not representative of the actual measured discontinuity sets in the field. Thus, judgement must be applied when using discontinuity sets extracted from TLS mapping, which must be confirmed through observation from field mapping.

Following the kinematic analysis, the potentially problematic planes/wedges for each slope were used as input parameters in the SMR classification of the slopes.

Rock Mass Rating

The assigned parameters and ratings of the three different RMR types – RMR₈₉, M-RMR, and RMR₁₄ – for each slope are given for all the discontinuities sets measured in the field, as shown in Figure 6. For each discontinuity set, the parameters for the RMR calculation are based on field mapping of the discontinuity tests and the results of the physico-mechanical properties from laboratory tests.

Based on the results, the majority of the RMR ratings assigned the Site 1-Site 3 slopes as class II slopes (RMR 61-80), or 'good', with the exception of the M-RMR for Site 1, which assigned the slope as class I (RMR 81-100), or 'very good'. By comparing the three RMRs, it was observed that RMR89 was consistently the most conservative, producing the lowest reading for all the discontinuity sets. On the other hand, the M-RMR calculation resulted in the highest values of RMR for each discontinuity set. This could be attributed to the M-RMR, which uses a continuous function (Sen & Sadagah, 2003) as opposed to the discrete ranking used in the other RMR, which aims to reduce subjectivity when assigning value to the RMR parameters. By assigning specific values to each parameter in the M-RMR, the calculation would lean more towards the higher range of each parameter's ranking. A similar comparative analysis of the RMR by Basahel & Mitri (2017) also noted that the continuous function of the RMR produced a higher value than other RMR ratings.

Slope Mass Rating

For the SMR calculation, the values from the RMR - RMR $_{89}$, M-RMR, RMR $_{14}$ - were all used as separate inputs for the different versions of the SMR – the original SMR, CSMR, and GSMR. In addition, the calculation of the SMR reading for each potential planar and wedge failure is based on the kinematic analysis for both the scanline mapping and TLS mapping discontinuities sets. The F_1 - F_3 parameters were determined using the discrete rating for the original SMR and the continuous rating for the CSMR. Meanwhile, the Ψ and F_3 parameters were determined graphically from the stereoplot created by Tomás $et\ al.\ (2012)$. The F_4 parameters for all the slopes were identified as smooth

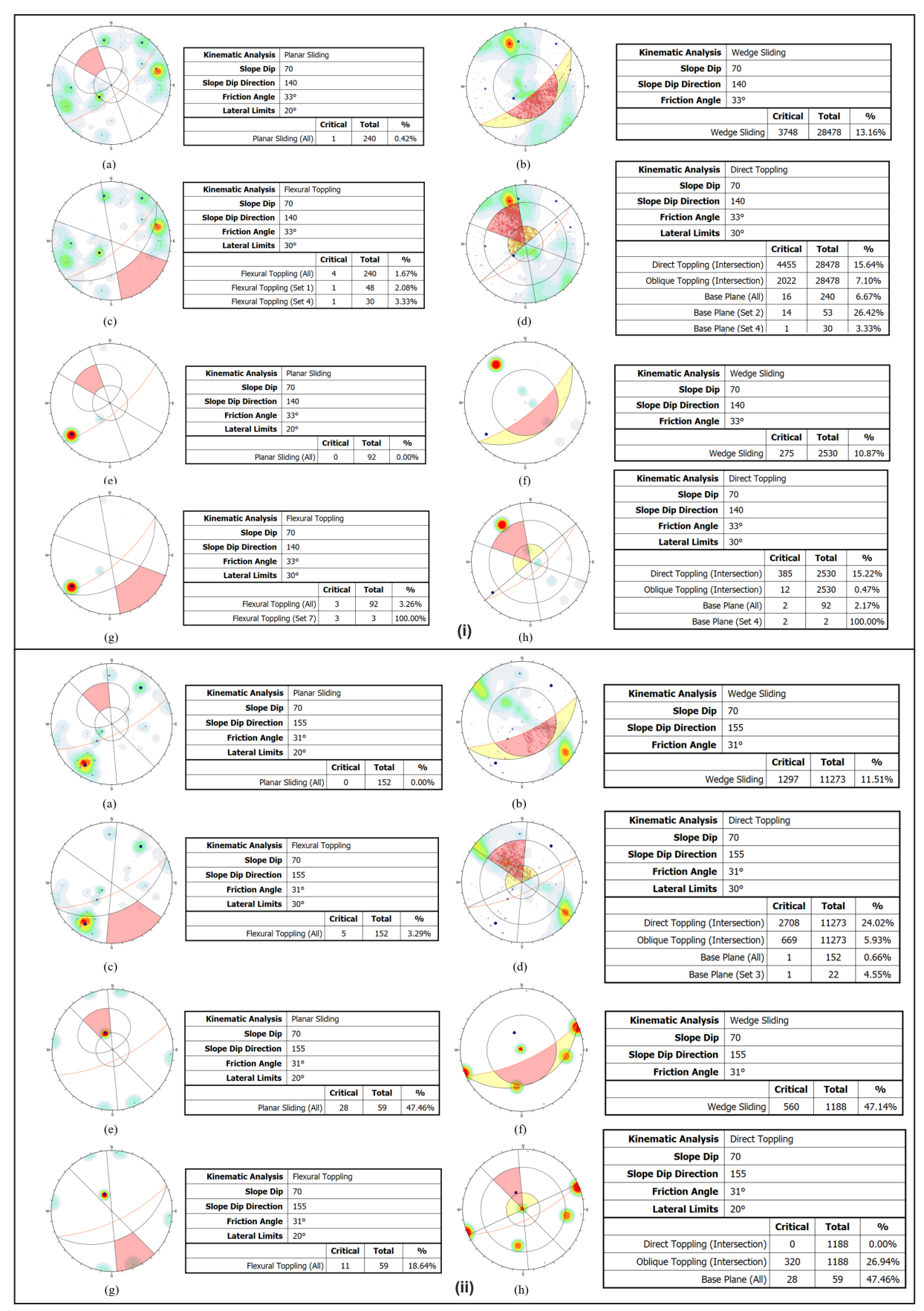


Figure 5: Kinematic analysis for: (i) Site 1, (ii) Site 2, and (iii) Site 3; (a) – (d) represent data from scanline mapping; (e) – (h) represent data from TLS mapping.

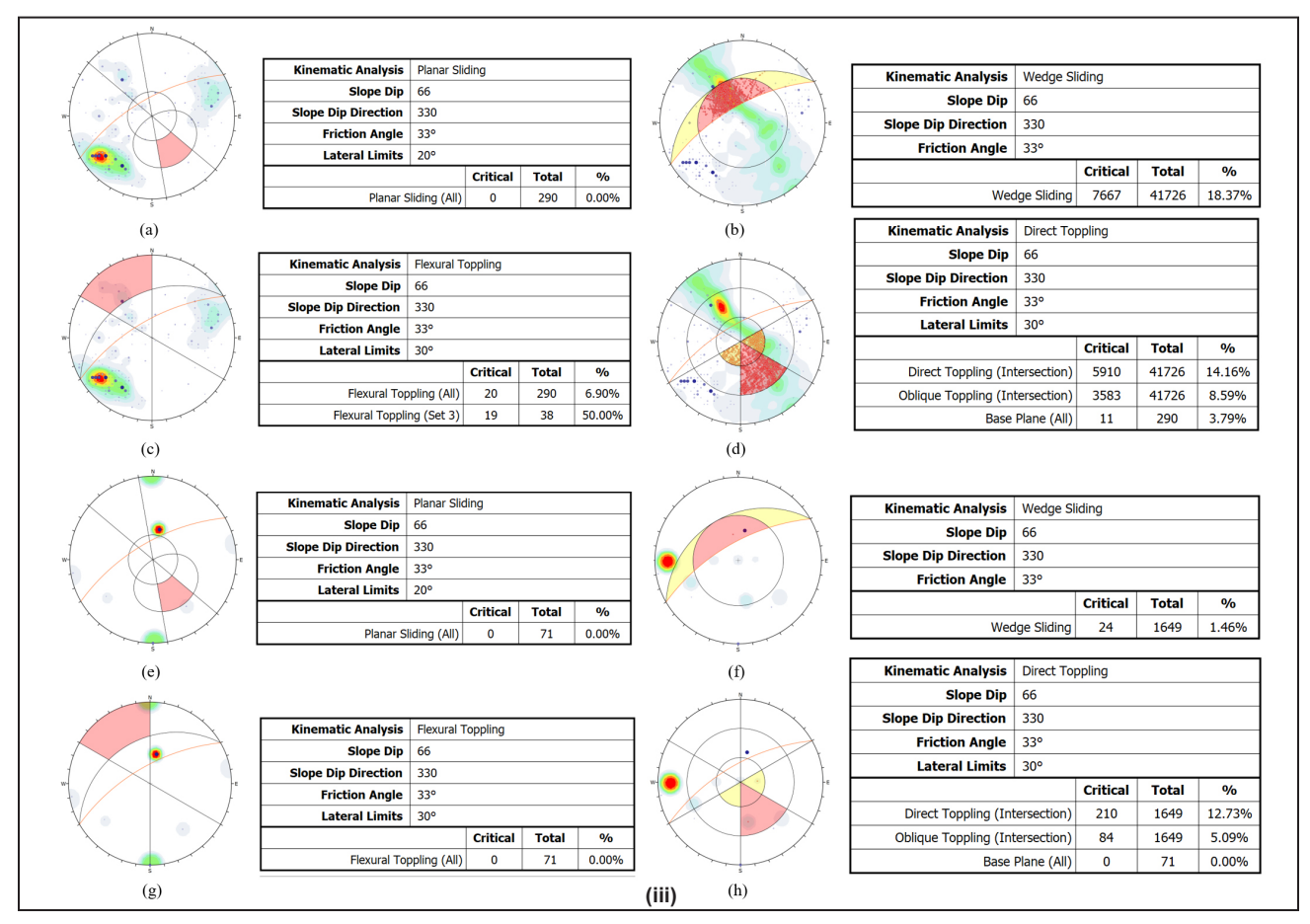


Figure 5: Continued.

Table 4: Potential mode of failure for Site 1-Site 3.

Slope	Planar failure (%)	Wedge failure (%)	Toppling fa	ailure (%)
Slope	Tianai ianuie (70)	weuge faiture (70)	Flexural	Direct
Site 1: Scanline mapping	0.42	13.16	1.67	15.64
Site 1: TLS mapping	0.00	10.87	3.26	15.22
Site 2: Scanline mapping	0.00	11.51	3.29	24.02
Site 2: TLS mapping	47.46	47.14	18.64	0.00
Site 3: Scanline mapping	0.00	18.37	6.90	14.16
Site 3: TLS mapping	0.00	1.46	0.00	12.73

blasting (+8). A summary of all the measured SMR values is shown in Figure 7.

For Site 1, the lowest SMR value was found in the wedge set (45°/140°) for scanline mapping and the wedge set (38°/131°) for TLS mapping. This would put the rock mass classification for those sets as Class IV and Class III, respectively, whereby they were classified as 'bad': unstable, with the potential for some planar or big wedge failures (60% probability), and 'normal': partially stable with the potential for some joint or many wedge failures (40% probability), respectively.

For Site 2, the lowest SMR value was found in the wedge set (50°/103°) for scanline mapping and the plane set (32°/156°) for TLS mapping. This would put the rock mass classification for those sets as Class II and Class IV, respectively, where they are classified as 'good', stable with potential for some blocks failure (20% probability), and 'bad', unstable with potential for some planar or big wedges failure (60% probability) respectively.

For Site 3, the lowest SMR value was found in the wedge set (36°/328°) for scanline mapping and the wedge

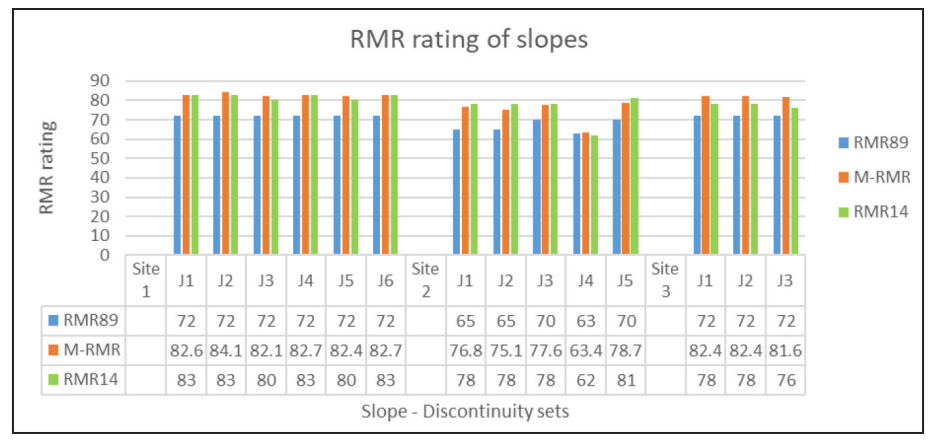


Figure 6: Graphical comparison of different RMR ratings for the slopes: RMR_{so}, M-RMR, RMR₁₄.

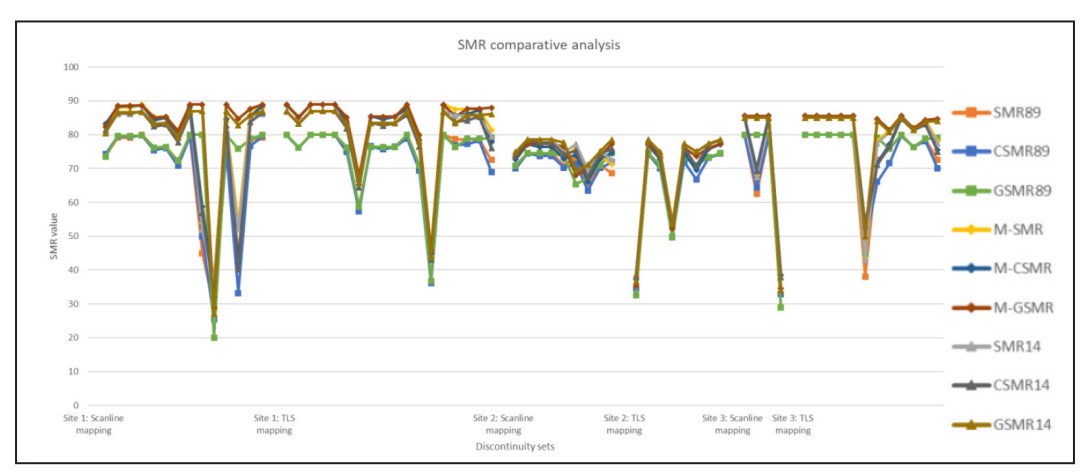


Figure 7: Graphical comparison of different SMR ratings for the slopes.

set (54°/349°) for TLS mapping. This would put the rock mass classification for those sets as Class IV and Class III respectively, whereby they were classified as 'bad': unstable with the potential for some planar or big wedge failures (60% probability), and 'normal': partially stable with the potential for some joint or many wedge failures (40% probability), respectively.

As discussed in the previous section on kinematic analysis, judgement is required when analysing discontinuity sets using TLS mapping. Therefore, only the SMR values using discontinuity sets from scanline mapping were used in the subsequent analysis of rock mass classifications. The Q-slope value is calculated by identifying a potentially unstable plane/wedge for each slope.

Q-slope method

For the calculation of the Q-slope, the most unfavourable discontinuity sets are used (i.e., the one with the lowest value from the SMR). As all the slopes indicated wedge failure as the most unfavourable discontinuity set, the two plane sets that formed the problematic wedge sets were used for the readings in Set A and Set B. For the J_{wice} and SRF_{slope}

parameters, the slope is described as stable and competent under a wet environment ($J_{\text{wice}} = 0.7$), and the overall slope condition is slightly loosening due to surface location, disturbance from blasting, or excavation (SRF_{slope} = 2.5). The value of the calculated Q-slope was plotted against the Q-slope stability chart developed by Bar & Barton (2017) (Figure 8), whereby it was found that Site 3 slope was stable, Site 1 slope was quasi-stable, and Site 2 slope was unstable.

Geological Strength Index

The GSI ratings in this study were evaluated using the various GSI quantifications, the purpose being to assign a single discrete reading for each studied slope. The evaluation of GSI_{95} and GSI_{13} was measured using parameters from RMR_{89} , and GSI_{02} was plotted graphically on the chart devised by Sonmez & Ulusay (2002) using the Surface Condition Rating (SCR) and Structure Rating (SR) parameters (Figure 9). Comparative analysis of the GSI values determined that GSI_{02} provided the lowest range of readings, whereas GSI_{13} provided the highest range of readings for each slope. With the value of GSI_{02} determined, the rating for the SSR was calculated.

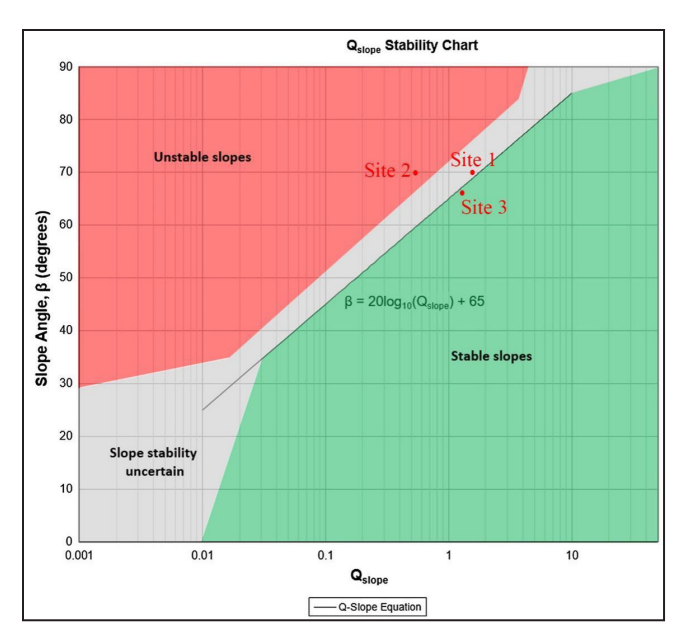


Figure 8: Q-slope stability chart of Site 1-Site 3. Chart modified from Bar & Barton (2017).

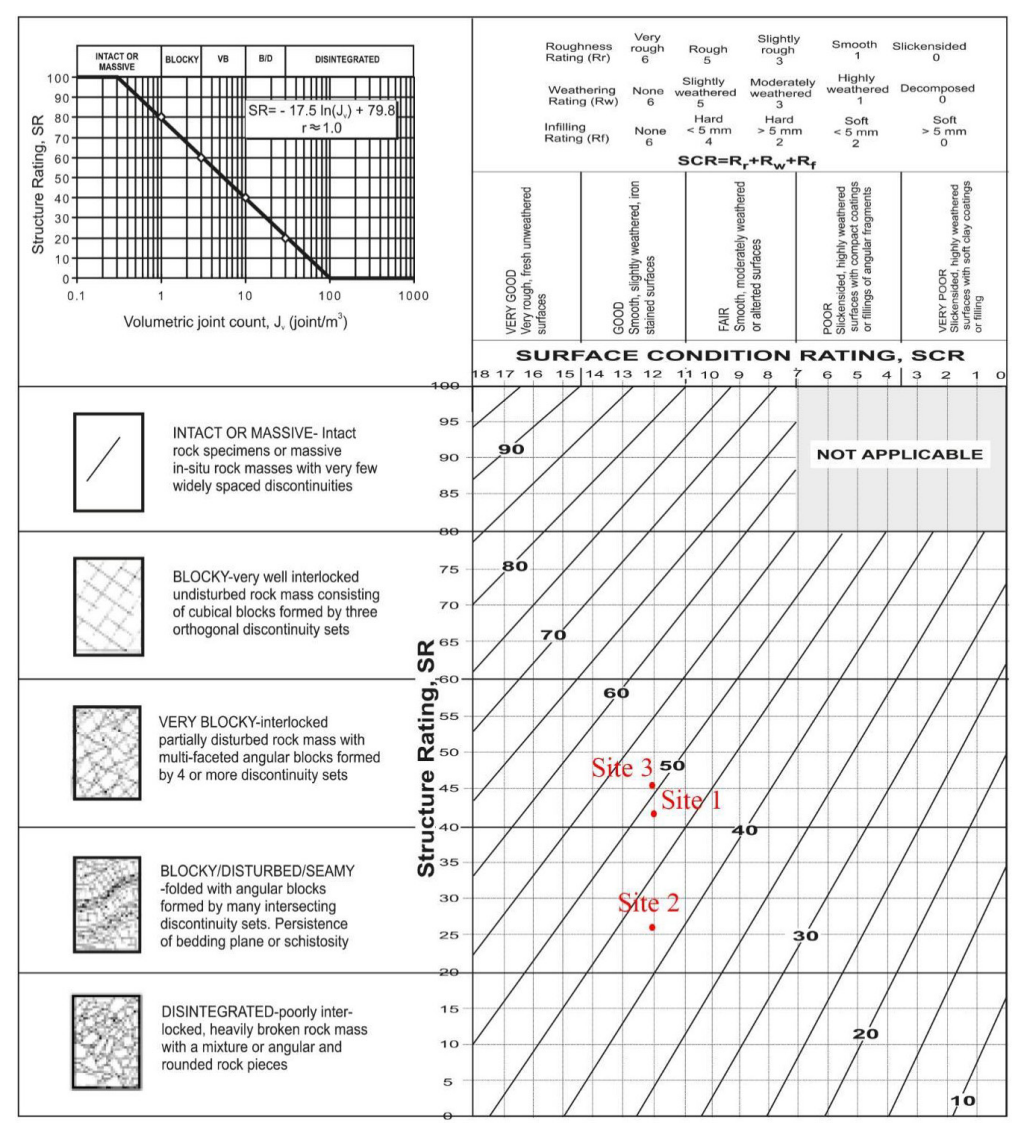


Figure 9: Estimation of the value of GSI₀₂ for Site 1-Site 3. Chart modified from Sonmez & Ulusay (2002).

Slope Stability Rating

The SSR was developed to consider the effect of additional parameters relating to the stability of slopes that were unavailable in the original GSI parameters. The system also provides a design chart entailing the stable angle of any slope height and the calculated SSR value. For this study, the proposed stable slope angle was used to validate the stability of the existing slopes. For all the slopes, the overall value of P_5 (the earthquake force rating) was assigned a value of 0, based on the seismic hazard map of the region (Jabatan Mineral dan Geosains, 2008) having a value of 2-3% g (0.02–0.03 g).

From the calculated SSR value, the readings were plotted on a set of design charts, representing the relationship between the slope height and SSR value against the safe slope angle – between 30° to 70° – and for a Factor of Safety (FoS) of

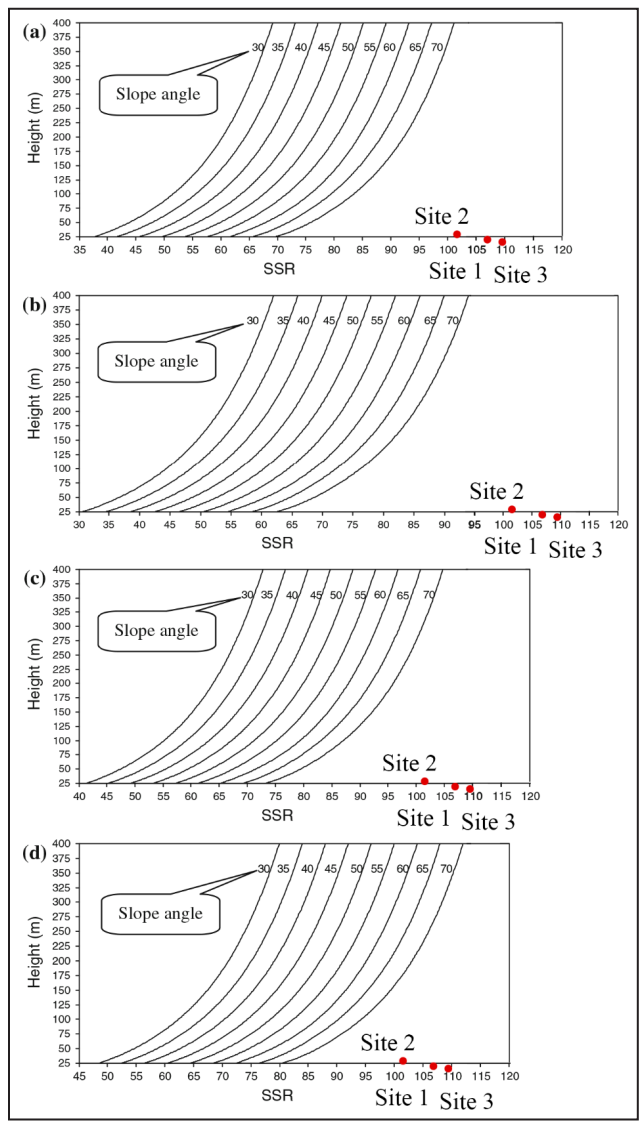


Figure 10: Plot of SSR rating of slopes overlaid on SSR design charts for different Factor of Safety (FoS). (a) - (d): FoS of 1.0, 1.2, 1.3, 1.5.

1.0, 1.2, 1.3, and 1.5 (Figure 10). By comparing this with the angle of the excavated slopes, all slopes were considered stable from the SSR design chart as the excavated slope angle meets the safe slope angle criterion for all the FoS ($>70^{\circ}$).

Hazard Index

The HI was developed to represent the hazard level of a rock slope failure. The first set of parameters for each slope – normal condition, $f_{\rm NC}$ – was calculated based on the identified potential failure modes. For the second set of parameters – triggering mechanism, $f_{\rm TM}$ – the value of $I_{\rm m}$ was based on the latest environmental statistics report on the area by the Department of Statistics Malaysia (2022), while the value of $I_{\rm cr}$ was 700 mm, based on the suggestion of Pantelidis (2010). Using the input parameters based on the most unstable joint sets determined from the kinematic analysis, the calculated HI values for all the slopes were 3.05, so they were assigned under the HI as 'good' quality (HI = 1–4).

DISCUSSION

The primary objective of the study was to characterise rock mass through conventional mapping and by applying TLS mapping of the rock slopes. For the latter, a 3D point model of the slopes and the extraction of the discontinuity sets orientation could be carried out through a semi-automated process. It was found that TLS mapping resulted in larger sets of datapoints compared to conventional scanline mapping, which was attributed to the method covering a larger surface area. In contrast, scanline mapping was limited to the lower sections of the accessible parts of the slopes. A comparison of the survey data related to the plotting of the discontinuity sets from the scanline and TLS mapping showed various degrees of correlation between the two datasets, ranging from strong and fair to weak correlations. The weak correlation of the discontinuity could be attributed to the persistence and continuity of the measured discontinuities, whereby the measured discontinuity at the lower section of a slope may not extend to the upper part, as well as being obscured by the weathering of rock mass (Hellmy et al., 2019). However, from this study, the method provided many more discontinuity datasets for stability analysis compared to conventional mapping. Various potential failure trends from the kinematic analysis were identified for all the mapped slopes. Thus, the potential for conducting kinematic analysis from TLS mapping was validated.

From the field mapping and laboratory tests, the majority of the rock surfaces of the slopes would fall into the categories of Grade II to Grade III, or slightly weathered rock to moderately weathered rock, respectively. Kinematic analysis using the mapped discontinuity sets indicated that the failure potential of the rock slopes was generally comparable, with the notable exception being the rock slope for Site 2, where the potential mode of failure obtained by scanline mapping and TLS mapping differed significantly. Considering the slope surface at Site 2 is covered by a

significant amount of weathered material, one explanation is that a significant weathering on the surface of a rock slope may have affected the extraction of discontinuity through TLS mapping, leading to the notably large discrepancy with kinematic analysis with regard to the data obtained through scanline mapping. Although TLS mapping can extract the parameters of discontinuity orientation – the dip and dip direction - other discontinuity parameters related to rock mass classification are still dependent on collection through field mapping. Any methodology available for extracting discontinuity parameters should be compared with field data for validation, and it should not be seen as a complete replacement for field measurement. For that reason, the application of TLS in slope stability analysis in this study was limited to kinematic analysis and the SMR for rock mass classification.

Following kinematic analysis, the rock mass classification of the slopes was determined. A summary of all the rock mass classifications for Site 1 to Site 3 is provided in Table 5. Under each of the different SMR, the three values represent the calculated SMR using the input of RMR₈₉, M-RMR, and RMR₁₄, respectively. For the classification of the rock slopes, the discrete function of RMR₈₉ provided the lowest range of values, compared to RMR₁₄ and the continuous function of M-RMR. This indicates that RMR₈₉ is the most conservative of the RMR ratings tested. This is reflected in the SMR classification, where SMR analysis using RMR_{so} exhibited the lowest range of values, and SMR analysis using M-RMR produced the highest range of values. Of the different SMR classifications, the plotting of the SMR and CSMR generally follows a similar trend across the different discontinuity sets. In contrast, the plotting of GSMR exhibited some deviations for certain discontinuity sets, which typically produced higher SMR values. This indicates how the adjustment factors of ψ and F_3 , which are calculated graphically, are subjected to greater subjectivity than the discrete rating of the correction factors for the original SMR or the continuous rating of the correction factors for the CSMR.

In addition to the SMR, slope classification using the Q-slope and HI is also based on the identification of potential modes of failure. The HI and GSI apply to non-structurally controlled slopes, i.e., heavily weathered slopes, or closely joined rock slopes. The Q-slope, SSR, and HI ratings indicate that most of the slopes were in stable condition, with Site 2 being potentially problematic (unstable from the Q-slope analysis, and blocky/disturbed/seamy rock mass from the GSI classification). It should also be noted how the HI rating indicates a similar rating for all the slopes, despite the differences in the potential failure modes for all the slopes. This would indicate how the relationship between discontinuity orientation and slope orientation, as well as triggering factors, are constant throughout the slopes in the area. Overall, kinematic analysis and rock mass classifications can validate the stability of existing

slopes, whereby slopes with low kinematic potential for failure are observed to correspond with higher values or classes of rock mass classifications. In contrast, slopes with significant kinematic potential for failure could be correlated with lower values or classes of rock mass classifications. It should be noted that this study only covers a small selection of slopes as a case study. It is recommended that a more extensive study of slopes should be carried out alongside a comparative analysis of rock mass classification to test the validity of and statistical relationships between the different rock mass classifications developed.

Finally, returning to the method of how the data were collected, it should be noted that field mapping and TLS mapping only cover the surficial aspect of rock mass. For rock mass in tropical conditions such as those in Malaysia, the weathering process and the presence of groundwater movement may internally alter the rock mass properties and act as triggers for slope failure, in addition to failure through discontinuity sets. Therefore, any comprehensive assessment of rock slopes should integrate geophysical surveys, such as electric resistivity, seismic, or ground penetrating radar surveys, to better identify a slope rock mass.

CONCLUSIONS

This study achieved the objective of utilising TLS to map discontinuity data for a rock slope stability analysis. A comparison of the survey data obtained using scanline mapping and TLS mapping of discontinuity revealed varying levels of correlation between the discontinuity datasets. Compared to the limited data acquisition from field mapping, TLS was able to map larger datasets of discontinuities, especially from the inaccessible upper zones of slopes. The discontinuity measurements were used for kinematic analysis and rock mass classifications. From the kinematic analysis, several potential modes of failure were identified. Comparative analysis was carried out between the use of discontinuities mapped using conventional scanline mapping and TLS mapping, which revealed the limitation of using TLS mapping on heavily weathered rock slopes. The use of discontinuity sets mapped from TLS for the SMR was also carried out, although the results were not as conclusive as those obtained from field mapping.

An assessment of the slopes was then carried out using several rock mass classification systems: the original RMR (RMR₈₉); the continuous function RMR, or the Modified-RMR (M-RMR); the 2014 RMR update (RMR₁₄), the original SMR; the continuous function SMR (CSMR); the graphical SMR (GSMR); the Q-slope system; the original GSI (GSI₉₅); the 2002 quantification of GSI (GSI₀₂); the 2013 quantification of GSI (GSI₁₃); the SSR; and the HI. By carrying out this comparative analysis, RMR₈₉ was found to produce the lowest rating of the RMR ratings; the original SMR and CSMR produced similar trends of readings, while the GSMR showed deviations for certain discontinuity sets; GSI₀₂ produced the lowest rating of the GSI ratings. Both

Table 5: Summary of rock mass classification for Site 1-Site 3. The values in (brackets) represent % of kinematic failure (for mode of failure) and classes (for RMR, SMR, and HI).

Site & mode of failures	RMR_{89}	M-RMR	\mathbf{RMR}_{14}	SMR	CSMR	GSMR	Q-slope	GSI_{95}	$\mathbf{GSI}_{_{02}}$	\mathbf{GSI}_{13}	SSR	H
Site 1	71.67 (II)	80.56 (I)	75.83 (II)					66.67	49	73.06	108	
Planar: 31°/51° (0.42%)				73.7/ 82.6/ 80.7 (I-II)	74.29/ 83.19/ 81.29 (I-II)	73.45/ 82.35/ 80.45 (I-II)						3.05 (good)
: ' ; ; ;				29/ 37.9/ 36 (IV)	25.50/ 34.40/ 32.50 (IV)	20.00/ 28.90/ 27.00 (TV)	1.68					3.05 (good)
Toppling: 72°/263° (1.67%)				76.25/ 85.15/ 83.25 (I-II)	75.41/ 84.31/ 82.41 (I-II)	76.18/ 85.08/ 83.18 (I-II)						3.05 (good)
Site 2	65 (II)	67.69 (II)	68.6 (II)					09	42.5	51.2	101.5	
410				65.6/ 68.29/ 69.6 (II)	63.50/ 66.19/ 67.50 (II)	67.10/ 69.79/ 71.10 (II)	0.54					3.05 (good)
Toppling: 75°/33° (3.29%)				70.85/ 73.54/ 74.85 (II)	70.00/ 72.69/ 74.00 (II)	70.85/ 73.54/ 74.85 (II)						3.05 (good)
Site 3	72.67 (II)	78.23 (II)	75.33 (II)					67.67	50.5	76.51	109.5	
Wedge: 36°/328° (18.37%)				29/ 34.56/ 34 (IV)	32.88/ 38.44/ 37.88 (TV)	29.00/ 34.56/ 34.00 (TV)	1.38					3.05 (good)
Toppling: 56°/135° (6.90%)				62.5/ 68.06/ 67.5 (II)	64.34/ 69.90/ 69.34 (II)	80.00/ 85.56/ 85.00 (I)						3.05 (good)

the Q-slope and SSR assessed the stability of the current slope design, with the former identifying an unstable slope for Site 2, a quasi-stable slope for Site 1, and a stable slope for Site 3. In contrast, the latter shows all the slopes falling within the range of stable slope angles. HI analysis found the slopes to share similar values of ratings, indicating that the relationship between discontinuity orientation and slope orientation for the slopes in the system is similar across the different slopes. Hence, the study achieved the objective of testing and validating the different rock mass classifications.

In conclusion, the study tested and confirmed the results of various rock mass classifications with the observed conditions of the rock slopes. Comparative analysis of the selected rock mass classifications results found them to be reliable for assessing the slope conditions. The overall assessment of the slopes found them to be mainly of good quality, with no immediate danger of failure. The stability of the slopes was validated by comparing the slope condition with the slope design for a stable slope angle.

ACKNOWLEDGEMENT

The authors would like to acknowledge the research support provided by Universiti Malaysia Pahang Al-Sultan Abdullah under the Geran Universiti Malaysia Pahang, grant number RDU190345, and the Postgraduate Research Grant Scheme, grant number PGRS2003207. We would also like to extend our gratitude to the reviewers and the editorial team for their constructive and insightful comments that have improved the quality of this manuscript.

AUTHORS CONTRIBUTION

AFS conducted the fieldwork, laboratory work, and data analysis of the mapped data with guidance from HA. HA managed the hardware acquisition and data processing for the TLS data and advised on data interpretation and manuscript writing.

CONFLICT OF INTEREST

The authors have no conflicts of interest to declare that are relevant to the content of this article.

REFERENCES

- Abdul Rahim, A.F., Md Rafek, A.G., Serasa, A.S., Jaapar, A.R., Goh, T.L., Roslee, R., Lee, K.E., Nguyen, X.H. & Tran, V.X., 2023. A Review of Rock Slope Stability Assessment Practice in Malaysia. Sains Malaysiana, 52(2), 399-416. DOI: 10.17576/jsm-2023-5202-07.
- Abdul Rahman, H. & Mapjabil, J., 2017. Landslides Disaster in Malaysia: An Overview. Health & the Environment Journal, 8(1), 58-71.
- Alejano, L.R., Muralha, J., Ulusay, R., Li, C.C., Pérez-Rey, I., Karakul, H., Chryssanthakis, P. & Aydan, Ö., 2018. ISRM Suggested Method for Determining the Basic Friction Angle of Planar Rock Surfaces by Means of Tilt Tests. Rock Mechanics and Rock Engineering, 51, 3853–3859. DOI: 10.1007/s00603-018-1627-6.
- Anbazhagan, S., Ramesh, V. & Saranaathan, S.E., 2017. Cut slope stability assessment along ghat road section of Kolli hills,

- India. Natural Hazards, 86(3), 1081–1104. DOI: 10.1007/s11069-016-2731-0.
- Awang, H., Salmanfarsi, A.F., Misbahuddi, A. Z. & Ali, M. I., 2021a. Slope stability analysis of rock mass using Rock Mass Rating and Slope Mass Rating. IOP Conference Series: Earth and Environmental Science, 682, 012015. DOI: 10.1088/1755-1315/682/1/012015.
- Awang, H., Salmanfarsi, A.F., Zaini, M.S.I., Mohamad Yazid, M. A.F., & Ali, M.I., 2021b. Investigation of groundwater table under rock slope by using electrical resistivity imaging at Sri Jaya, Pahang, Malaysia. IOP Conference Series: Earth and Environmental Science, 682, 012017. DOI: 10.1088/1755-1315/682/1/012017.
- Bar, N. & Barton, N., 2017. The Q-Slope Method for Rock Slope Engineering. Rock Mechanics and Rock Engineering, 50(12), 3307–3322. DOI: 10.1007/s00603-017-1305-0.
- Barton, N. & Bar, N., 2015. Introducing the Q-slope method and its intended use within civil and mining engineering projects. In:
 W. Schubert & A. Kluckner (Eds.), Future Development of Rock Mechanics: Proceedings of the ISRM Regional Symposium EUROCK 2015 & 64th Geomechanics Colloquium; October 7-10, 2015, Salzburg, Austria. Österreichische Gesellschaft für Geomechanik, Salzburg, 157–162.
- Basahel, H. & Mitri, H., 2017. Application of rock mass classification systems to rock slope stability assessment: A case study. Journal of Rock Mechanics and Geotechnical Engineering, 9, 993–1009. DOI: 10.1016/j.jrmge.2017.07.007.
- Battulwar, R., Zare-Naghadehi, M. Emami, E. & Sattarvand, J., 2021. A state-of-the-art review of automated extraction of rock mass discontinuity characteristics using threedimensional surface models. Journal of Rock Mechanics and Geotechnical Engineering, 13(4), 920–936. DOI: 10.1016/j. jrmge.2021.01.008.
- Bieniawski, Z.T., 1973. Engineering classification of jointed rock masses. Civil Engineer in South Africa, 15(12), 335-343.
- Bieniawski, Z.T., 1976. Exploration for rock engineering. In: A.A. Balkema (Ed.), Proceedings of the Symposium on exploration for rock engineering, Cape Town, South Africa.
- Bieniawski, Z.T., 1979. The geomechanics classification in rock engineering applications. Proceedings of the 4th International Congress on Rock Mechanics, Montreux, 41–48.
- Bieniawski, Z.T., 1989. Engineering rock mass classifications: a complete manual for engineers and geologists in mining, civil, and petroleum engineering. John Wiley & Sons, New York. 250 p.
- Bieniawski, Z.T., 1993. Classification of rock masses for engineering: The RMR system and future trends. In: Hudson, J.A. (Ed.), Comprehensive Rock Engineering, Vol. 3: Rock Testing and Site Characterization - Principles, Practice & Projects. Pergamon Press, New York, 553-573.
- Bordehore, L.J., Riquelme, A., Cano, M. & Tomás, R., 2017. Comparing manual and remote sensing field discontinuity collection used in kinematic stability assessment of failed rock slopes. International Journal of Rock Mechanics and Mining Sciences, 97, 24-32. DOI: 10.1016/j.ijrmms.2017.06.004.
- British Standards Institution, 2015. Code of Practice for Site Investigations. BS 5930: 2015+A1:2020. BSI, London. 328 p.
- British Standards Institution, 2018. Geotechnical investigation and testing. Identification, description and classification of rock. Part 1: Identification and description. BS EN ISO 14689:2018. BSI, London. 28 p.

- Celada, B., Tardáguila, I., Varona, P., Rodríguez, A. & Bieniawski, Z. T., 2014. Innovating tunnel design by an improved experience-based RMR system. In: A. Negro, M.O. Cecilio Jr. & W. Bilfinger (Eds.), Proceedings of the World Tunnel Congress. CBT/ABMS, Brazil, 1–9.
- Cobbing, E.J., Pitfield, P.E.J., Darbyshire, D.P.F. & Mallick, D.I.J., 1992. The granites of the South-East Asian tin belt. HMSO, London. 369 p.
- Department of Statistics Malaysia, 2022. Environment Statistics 2022 Pahang. Department of Statistics Malaysia, Putrajaya. 90 p.
- Fookes, P.G., 1997. Tropical Residual Soils. The Geological Society London, London. 184 p.
- Gasparon, M. & Varne, R., 1995. Sumatran granitoids and their relationship to Southeast Asian terranes. Tectonophysics, 251, 277–299. DOI: 10.1016/0040-1951(95)00083-6.
- Ghani, A.A., Shahjamal, M., Ng, T.F., Ismail, N.E.H., Mohamad Zulkifley, M.T, Islami, N., Quek, L.X., Abu Bakar, A.F., Hassan, M.H.A., Abdul Aziz, J.H. & Masor, A.F., 2019. Ce Anomaly in I–Type Granitic Soil from Kuantan, Peninsular Malaysia: Retention of Zircon in the Weathering Product. Sains Malaysiana, 48(2), 309–315. DOI: 10.17576/jsm-2019-4802-06.
- Hack, R., Price, D. & Rengers, N., 2003. A new approach to rock slope stability-a probability classification (SSPC). Bulletin of Engineering Geology and the Environment, 62(2), 167-184. DOI: 10.1007/s10064-002-0155-4.
- Hellmy, M.A.A., Muhammad, R. F., Shuib, M.K., Ng, T. F., Abdullah, W.H., Abu Bakar, A. & Kugler, R., 2019. Rock Slope Stability Analysis based on Terrestrial LiDAR on Karst Hills in Kinta Valley Geopark, Perak, Peninsular Malaysia. Sains Malaysiana, 48(11), 2595–2604. DOI: 10.17576/jsm-2019-4811-29.
- Highland, L.M. & Bobrowsky, P., 2008. The landslide handbook—A guide to understanding landslides. United States Geological Survey, Reston. 147 p.
- Hoek, E., 2007. Rock mass properties. Practical rock engineering. www.rocscience.com/learning/hoek-s-corner.
- Hoek, E. & Bray, J.W., 1981. Rock Slope Engineering. Institute of Mining and Metallurgy, London. 456 p.
- Hoek, E., Carter, T.G. & Diederichs, M.S., 2013. Quantification of the Geological Strength Index Chart. In: L.J. Pyrak-Nolte (Ed.), 47th US Rock Mechanics / Geomechanics Symposium, San Francisco, CA, USA, June 23-26. American Rock Mechanics Association, Virginia. 3116 p.
- Hoek, E., Kaiser, P.K. & Bawden, W.F., 1995. Support of Underground Excavations in Hard Rock. Balkema, Rotterdam. 235 p.
- Ismail, A., Ahmad Safuan, A.R., Sa'aari, R., Rasib, A.W., Mustaffar, M., Abdullah, R.A., Kassim, A., Mohd Yusof, N., Abd Rahaman, N. & Kalatehjari, R., 2022. Application of combined terrestrial laser scanning and unmanned aerial vehicle digital photogrammetry method in high rock slope stability analysis: A case study. Measurement, 195, 111161. DOI: 10.1016/j. measurement.2022.111161.
- Jabatan Mineral dan Geosains, 2008. Assessment of the Seismic Threats to Malaysia from Major Earthquakes in the Southeast Asian Region: Seismic and Tsunami Hazards and Risks Study in Malaysia. Minerals and Geoscience Department, Kuala Lumpur. 122 p.
- Khanna, R. & Dubey, R.K., 2021. Comparative assessment of slope stability along road-cuts through rock slope classification systems in Kullu Himalayas, Himachal Pradesh, India. Bulletin

- of Engineering Geology and the Environment, 80, 993–1017. DOI: 10.1007/s10064-020-02021-4.
- Komoo, I., 1995. Weathering as an important factor in assessing engineering proper-ties of rock material. Forum on Soil and Rock Properties. Geological Society of Malaysia, Universiti Malaya, Kuala Lumpur, 31–35.
- Kundu, J., Sarkar, K., Tripathy, A., & Singh, T. N., 2017. Qualitative stability assessment of cut slopes along the National Highway-05 around Jhakri area, Himachal Pradesh, India. Journal of Earth System Science, 126(8), 112. DOI: 10.1007/ s12040-017-0893-0.
- Nagendran, S.K., Mohamad Ismail, M.A. & Wen, Y., 2019. 2D And 3D Rock Slope Stability Assessment Using Limit Equilibrium Method Incorporating Photogrammetry Technique. Bulletin of the Geological Society of Malaysia, 68, 133–139. DOI: 10.7186/bgsm68201913.
- Nugraheni, R.D., Sunjaya, D. & Agustini, S., 2018. Regional tectonic and geochemical approach to distinguish bauxite characteristics in Pahang, Malaysia and West Kalimantan, Indonesia. IOP Conference Series: Earth and Environmental Science, 212, 012026. DOI: 10.1088/1755-1315/212/1/012026.
- Pantelidis, L., 2009. Rock slope stability assessment through rock mass classification systems. International Journal of Rock Mechanics and Mining Sciences, 46(2), 315-325. DOI: 10.1016/j.ijrmms.2008.06.003.
- Pantelidis, L., 2010. An alternative rock mass classification system for rock slopes. Bulletin of Engineering Geology and the Environment, 69(1), 29-39. DOI: 10.1007/s10064-009-0241-y.
- Papathanassiou, G., Riquelme, A., Tzevelekis, T. & Evaggelou, E., 2020. Rock Mass Characterization of Karstified Marbles and Evaluation of Rockfall Potential Based on Traditional and SfM-Based Methods; Case Study of Nestos, Greece. Geosciences, 10(10), 389. DOI: 10.3390/geosciences10100389.
- Price, N. J. & Cosgrove, J.W., 1990. Analysis of geological structures. Cambridge University Press, Cambridge. 502 p.
- Public Work Department, 2009. National Slope Master Plan Sectoral Report Research and Development. Jabatan Kerja Raya Malaysia, Kuala Lumpur.
- Riquelme, A.J., Abellán, A., Tomás, R. & Jaboyedoff, M., 2014. A new approach for semi-automatic rock mass joints recognition from 3D point clouds. Computers & Geosciences, 68, 38-52. DOI: 10.1016/j.cageo.2014.03.014.
- Riquelme, A., Tomás, R. & Abellán, A., 2016. Characterization of rock slopes through slope mass rating using 3D point clouds. International Journal of Rock Mechanics and Mining Sciences, 84, 165–176. DOI: 10.1016/j.ijrmms.2015.12.008.
- Rocscience Inc., 2014. Dip v. 6.0 graphical and statistical analysis of orientation data. Toronto, Canada.
- Romana, M., 1985. New adjustment ratings for application of Bieniawski classification to slopes. Proceedings of International Symposium on the Role of Rock Mechanism, Zacatecas, 49-53.
- Romana, M., Tomás, R. & Serón, J.B., 2015. Slope Mass Rating (SMR) geomechanics classification: thirty years review. 13th ISRM International Congress of Rock Mechanics, 10-13 May, Montreal, Canada.
- Roslan, R., Che Omar, R., Baharuddin, I.N.Z., Abdul Wahab, W. & Buslima, F.S., 2019. Discontinuity Mapping using Terrestrial Laser Scanner and Kinematic Method. International Journal of Engineering and Advanced Technology, 9(1), 3640–3644. DOI: 10.35940/ijeat.A2704.109119.
- Sardana, S., Verma, A.K., Singh, A. & Laldinpuia, 2019.

- Comparative analysis of rockmass characterization techniques for the stability prediction of road cut slopes along NH-44A, Mizoram, India. Bulletin of Engineering Geology and the Environment, 78(8), 5977–5989. DOI: 10.1007/s10064-019-01493-3.
- Schwartz, M.O., Rajah, S.S., Askury, A.K., Putthapiban, P. & Djaswadi, S., 1995. The Southeast Asian Tin Belt. Earth Science Reviews, 38, 95-293. DOI: 10.1016/0012-8252(95)00004-T.
- Şen, Z. & Sadagah, B.H., 2003. Modified rock mass classification system by continuous rating. Engineering Geology, 67(3-4), 269-280. DOI: 10.1016/S0013-7952(02)00185-0.
- Simon, N., Mat Akhir, J., Napiah, A. & Tan, H.K., 2008. Development of landslide database along km 160 km 190, East Coast Highway, Pahang. Warta Geologi, 34 (5&6), 233–238.
- Sonmez, H. & Ulusay, R., 2002. A discussion on the Hoek-Brown failure criterion and suggested modifications to the criterion verified by slope stability case studies. Yerbilimleri, 26, 77–99.
- Sturzenegger, M. & Stead, D., 2009. Quantifying discontinuity orientation and persistence on high mountain rock slopes and large landslides using terrestrial remote sensing techniques. Engineering Geology, 106(3-4), 163-182. DOI: 10.1016/j. enggeo.2009.03.004.
- Taheri, A. & Tani. K., 2010. Assessment of the slope stability of rock slopes by slope stability rating classification system. Rock Mechanics and Rock Engineering, 43(3), 321–333. DOI: 10.1007/s00603-009-0050-4.
- Tan, B.K., 2017. Engineering geology in Malaysia some case studies. Bulletin of the Geological Society of Malaysia, 64,

- 65-79. DOI: 10.7186/bgsm64201707.
- Tan, H.K., Mat Akhir, J., Napiah, A. & Simon, N., 2008. Pemetaan ramalan potensi tanah runtuh di sepanjang km160-190 Lebuhraya Pantai Timur dengan pendekatan Sistem Maklumat Geografi: Kaedah statistik. Warta Geologi, 34 (5&6), 239–242.
- Tate, R.B., Tan, D.N.K. & Ng, T.F., 2008. Geological Map of Peninsular Malaysia. Scale 1:1 000 000. Geological Society of Malaysia & University Malaya.
- Tomás, R., Delgado, J. & Seron, J.B., 2007. Modification of slope mass rating (SMR) by continuous functions. International Journal of Rock Mechanics and Mining Sciences, 44(7), 1062-1-69. DOI: 10.1016/j.ijrmms.2007.02.004.
- Tomás, R., Valdes-Abellan, J., Tenza-Abril, A.J. & Cano, M., 2012. New insight into the slope mass rating geomechanical classification through four-dimensional visualization. International Journal of Rock Mechanics and Mining Sciences, 53, 64-69. DOI: 10.1016/j.ijrmms.2012.04.002.
- Ulusay, R., 2015. The ISRM Suggested Methods for Rock Characterization, Testing and Monitoring: 2007-2014. Springer International Publishing, Switzerland. 293 p.
- Ulusay, R. & Hudson, J.A., 2007. The complete ISRM suggested methods for rock characterization, testing and monitoring: 1974-2006. International Society of Rock Mechanics Commission on Testing Methods, 2007, Ankara. 628 p.
- Zaini, M.S.I., Hasan, M., & Zolkepli, M.F., 2022. Urban landfills investigation for leachate assessment using electrical resistivity imaging in Johor, Malaysia. Environmental Challenges, 6, 100415. DOI: 10.1016/j.envc.2021.100415.

APPENDIX

Table A: Evaluation of RMR for Site 1-Site 3.

Discontinuity	R_{δ}	$R_{_{RQD}}$	R_{SD}	R_{CD}	R _{CD14}	$\mathbf{R}_{_{\mathrm{IRA}}}$	R_{cg}	RMR_{89}	M-RMR	RMR_{14}
				·	Site 1					
J1	7	15	15	20	17	10	15	72	80.68	79
J2	7	15	15	20	17	10	15	72	82.27	79
J3	7	15	15	20	17	10	15	72	80.19	79
J4	7	15	15	20	17	10	15	72	80.87	79
J5	7	15	15	20	17	10	15	72	80.49	79
J6	7	15	15	20	17	10	15	72	80.87	79
Average								72	80.90	79
					Site 2					
J1	7	12	10	21	15	10	15	65	71.81	69
J2	7	12	10	21	15	10	15	65	70.05	69
J3	7	12	15	21	15	10	15	70	72.59	74
J4	7	12	8	21	15	10	15	63	58.38	67
J5	7	12	15	21	15	10	15	70	73.65	74
Average								66.67	69.29	70.6
					Site 3					
J1	7	20	10	20	15	10	15	72	77.83	77
J2	7	20	10	20	15	10	15	72	77.83	77
J3	7	20	10	20	15	10	15	72	77.03	77
Average								72	77.56	77

Table B: Classification of SMR for Site 1-Site 3.

Slope	SMR89 range	M-SMR range	SMR14 range	CSMR89 range	M-CSMR range	CSMR14 range	GSMR89 range	M-GSMR range	GSMR14 range	Class	Stability	Potential failure
C* 1												planes
Site 1: sca												
Planar	73.7-80	82.6-	80.7-87	74.29-	83.19-	81.29-	73.45-	82.35-	80.45-	II	Stable	31°/51°
		88.9		79.74	88.64	86.74	79.74	88.64	86.74			
Toppling	76.25	85.15	83.25	75.41	84.31	82.41	76.18	85.08	83.18	II	Stable	72°/263°
Wedge	29-79.1	37.9-88	36-86.1	25.50-	34.40-	32.50-	20.00-	28.90-	27.00-	IV	Unstable	45°/140°
				79.60	88.50	86.60	80.00	88.90	87.00			
Site 1: TL	S mappin	g										
Planar	80	88.90	87	80	88.90	87	80	88.90	87	I	Complete-	No
							• · · · · · · · · · · · · · · · · · · ·			•	ly stable	failures
Toppling	58.75-	67.65-	65.75-	76.16-	85.06-	83.16-	76.25-	85.15-	83.25-	III	Partially	68°/312°
	80	88.9	87	79.90	88.80	86.90	80.00	88.90	87.00	******************	stable	
Wedge	36.65-	45.55-	43.65-	36.07-	44.97-	43.07-	36.80-	45.70-	43.80-	IV	Unstable	38°/131°
	80	88.9	87	79.77	88.67	86.77	80.00	88.90	87.00			
Site 2: sca	ınline map	ping										
Planar	74.6	77.29	78.6	74.6	77.29	78.6	74.6	77.29	78.6	II	Stable	No
												failures
Toppling	70.85-	73.54-	74.85-	70.00-	72.69-	74.00-	70.85-	73.54-	74.85-	II	Stable	75°/33°
	74.6	77.29	78.6	74.50	77.19	78.50	74.60	77.29	78.60			
Wedge	65.6-	68.29-	69.6-	63.50-	66.19-	67.50-	65.40-	68.09-	69.40-	II	Stable	50°/103°
	73.25	75.94	77.25	71.92	74.61	75.92	74.60	77.29	78.60			
Site 2: TL	S mappin	g	-									
Planar	32.6-	35.29-	36.6-	34.54-	37.23-	38.54-	32.60-	35.29-	36.60-	IV	Unstable	32°/156°
	74.6	77.29	78.6	74.32	77.01	78.32	74.60	77.29	78.60			
Toppling	49.6-	52.29-	53.6-	49.73-	52.42-	53.73-	49.60-	52.29-	53.60-	III	Partially	87°/338°
	70.85	73.54	74.85	69.98	72.67	73.98	70.85	73.54	74.85		stable	
Wedge	71-74.6	73.69-	75-78.6	66.83-	69.52-	70.83-	71.00-	73.69-	75.00-	II	Stable	27°/188°
		77.29		74.43	77.12	78.43	74.60	77.29	78.60			
Site 3: sca	ınline mar	oning										
Planar	80	85.56	85	80	85.56	85	80.00	85.56	85.00	I	Complete-	No
. 141141	00	05.50	0.5	30	05.50	33	30.00	05.50	33.00	1	ly stable	failures
Toppling	62.5	68.06	67.5	64.34	69.90	69.34	80.00	85.56	85.00	ш	Stable	56°/135°
	• • • • • • • • • • • • • • • • • • • •		• • • • • • • • • • • • • • • • • • • •	•••••				• • • • • • • • • • • • • • • • • • • •	• • • • • •			
Wedge	29	34.56	34	32.88	38.44	37.88	29.00	34.56	34.00	IV	Unstable	36°/328°
	S mappin	-	0.7		0.5.5.6			0.5.5.6	0.5		G 1:	
Planar	80	85.56	85	80	85.56	85	80	85.56	85	I	Complete-	No
				•		• • • • • • • • • • • • • • • • • • • •	• • • • • • • • • • • • • • • • • • • •		• • • • • • • • • • • • • • • • • • • •		ly stable	failures
Toppling	80	85.56	85	80	85.56	85	80	85.56	85	I	Complete-	No
										•	ly stable	failures
Wedge	38-80	43.56-	43-85	48.04-	53.60-	53.04-	45.00-	50.56-	50.00-	IV	Unstable	54°/349°
		85.56		79.72	85.28	84.72	80.00	85.56	85.00			

AHMAD FAIZ SALMANFARSI, HARYATI AWANG

Table C: Evaluation of Q-slope for Site 1-Site 3.

Site 1	RQD	Unstable plane/ wedge: 45°/140°	J_{n}	\mathbf{J}_{r}	$\mathbf{J}_{_{\mathbf{a}}}$	O-factor	$\mathbf{J}_{\mathrm{wice}}$	$\mathrm{SRF}_{\mathrm{slope}}$	Q-slope
Set A	87.10	78°/64°	12	1	1	0.75	0.7	2.5	1.52
Set B	87.10	81°/222°	12	1	1	0.9	0.7	2.5	1.83
Average						-			1.68
Site 2	RQD	Unstable plane/ wedge: 50°/103°	J_n	J_r	J_{a}	O-factor	$\mathbf{J}_{\mathrm{wice}}$	SRF _{slope}	Q_{slope}
Set A	44.20	75°/33°	15	1	1	0.5	0.7	2.5	0.41
Set B	44.20	78°/178°	15	1	1	0.8	0.7	2.5	0.66
Average									0.54
Site 3	RQD	Unstable plane/ wedge: 36°/328°	J_n	J_{r}	Ja	O-factor	$\mathbf{J}_{\mathrm{wice}}$	SRF _{slope}	Q _{slope}
Set A	91.01	73°/45°	12	1	1	0.5	0.7	2.5	1.06
Set B	91.01	71°/253°	12	1	1	0.8	0.7	2.5	1.70
Average									1.38

Table D: Evaluation of GSI for Site 1-Site 3.

Site	RMR ₈₉	R _r	R _w	R_{f}	J_{v}	SCR	SR	R _{CD}	RQD	GSI ₉₅	GSI ₀₂	GSI ₁₃
Site 1	72	1	5	6	8.45	12	42.44	20	87.1	67	49	73.55
Site 2	66.6	1	5	6	21.45	12	26.15	21	44.2	61.6	42.5	53.6
Site 3	72	1	5	6	7.27	12	45.09	20	91.01	67	50.5	75.51

Table E: Evaluation of SSR for Site 1.

Site	\mathbf{GSI}_{02}	$\mathbf{P}_{_{1}}$	\mathbf{P}_{2}	$\mathbf{P}_{_{3}}$	$\mathbf{P}_{_{4}}$	\mathbf{P}_{5}	SSR
Site 1	49	28	25	6	0	0	108
Site 2	42.5	28	25	6	0	0	101.5
Site 3	50.5	28	25	6	0	0	109.5

Table F: Stability condition of slopes estimated from SSR design charts.

Site	SSR rating	Slope height	Slope angle	Calculate	d safe slope a	ngle from des	ign charts	Stability
Site	SSK rating	(m)	(°)	FoS = 1.0	FoS = 1.2	FoS = 1.3	FoS = 1.5	Stability
Site 1	108	21	70	>70°	>70°	>70°	>70°	Stable
Site 2	101.5	28	70	>70°	>70°	>70°	>70°	Stable
Site 3	109.5	18	66	>70°	>70°	>70°	>70°	Stable

Table G: Evaluation of HI for Site 1-Site 3.

Site and mode of failure	$\mathbf{f}_{_{1}}$	$\mathbf{f_2}$	$\mathbf{f}_{ ext{NC}}$	I_{m}	I_{cr}	$\mathbf{f}_{_{\mathrm{D}}}$	\mathbf{f}_{TM}	НІ
Site 1								
Planar: 31°/51°	10	1	1	2167.9	700	3	9.291	3.05
Toppling: 72°/263°	10	1	1	2167.9	700	3	9.291	3.05
Wedge: 45°/140°	10	-	1	2167.9	700	3	9.291	3.05
Site 2								
Toppling: 75°/33°	10	1	1	2167.9	700	3	9.291	3.05
Wedge: 50°/103	10	-	1	2167.9	700	3	9.291	3.05
Site 3								
Toppling: 56°/135°	10	1	1	2167.9	700	3	9.29	3.05
Wedge: 36°/328°	10	-	1	2167.9	700	3	9.29	3.05

Manuscript received 13 June 2024; Received in revised form 22 September 2024; Accepted 20 February 2025 Available online 28 November 2025